ARTICLE

Synthesis, Crystal and Electronic Structure of Layered *AM*Sb Compounds (*A* = Rb, Cs; *M* = Zn, Cd)

Bryan Owens-Baird,[a,b] Lin-Lin Wang,[b] Shannon Lee,[a,b] and Kirill Kovnir*[a,b]

Dedicated to Professor Yuri Grin on the occasion of his 65th birthday

Abstract: Synthesis, crystal structure, thermal stability, and electronic band structure of four new metal antimonides *AM*Sb (*A* = Rb, Cs; *M* = Zn, Cd) are reported. CsZnSb and RbZnSb crystallize in the hexagonal ZrBeSi structure type, in a $P6_3/mmc$ space group (No. 194, $Z = 2$) and unit cell dimensions of $a = 4.5588(2)/4.5466(4)$ Å and $c = 11.9246(6)/11.0999(10)$ Å. CsCdSb and RbCdSb crystallize in the tetragonal PbFCl structure type in a $P4/nmm$ space group (No. 129; $Z = 2$) and unit cell parameters of $a = 4.8884(5)/4.8227(3)$ Å and $c = 8.8897(9)/8.5492(7)$ Å. All four compounds are air- and water-sensitive and are shown through DSC measurements to decompose between 975 K and 1060 K. Analysis of the calculated electronic band structure shows that the Zn-containing antimonides are topologically trivial narrow bandgap semiconductors, while Cd-containing compounds exhibit a band inversion along $\Gamma - Z$ direction.

Introduction

Metal antimonides have been shown over the years to possess a wide range of flexible and interesting structures. These include binary, ternary, and multinary structures that range from simple 0-D to complex 3-D motifs.[1-6] Because of this, metal antimonides have found themselves at the forefront of many applications, such as thermoelectrics, photodetectors, LEDs, integrated circuits, and others.[7-11] A notable example is the well-known $Yb_{14}MnSb_{11}$, which has been identified as an efficient high-temperature *p*-type leg for thermoelectric generators.[11-13]

Examining the reported compounds in the ternary alkali metal–antimonide systems, two things become apparent: *i)* there is a high number of compounds with 111 stoichiometry that crystallize in extraordinarily common ZrBeSi or PbFCl structure types; and *ii)* that a large number of these compounds are found for the lighter alkali metals (Li, Na, or K) while the heavier metals (Rb or Cs) are underrepresented.[14-15] The latter point is not as easily explained. It may be due to fundamental issue that the size of the largest cations makes their ternary compounds less stable. Practical challenges in containing of highly reactive Rb and Cs at the elevated temperatures in the reaction vessels that are compatible with other components may have also sequestered research using these metals. For example, at 873 K Cs and Rb violently react with silica ampoule, while melts containing Sb react with Nb and Ta ampoule material at this temperature.

Some of the *ABX* compounds that crystallize in the ZrBeSi or PbFCl structure types have exhibited or been predicted to show interesting topological properties.[16-21] These unusual electronic band structures have jumpstarted a large investigation into topological materials, their observed properties, and their potential uses in advanced electronics. In 2012, *Zhang et al.* published a large computational study predicting many unreported 111 *ABX* structures, attempting to sort the relative stabilities of the hypothetical compounds.[22] Two of the most predicted structure types in this study were the ZrBeSi and PbFCl structure types. Among many compositions investigated in this report, they examined the hypothetical compositions RbZnSb and RbCdSb, concluding both to be energetically stable and should be synthetically achievable. Cs based compounds, however, were not explored in this study.

In this work, we present four new compounds: CsZnSb, RbZnSb, CsCdSb, and RbCdSb. The Zn-containing compounds crystallize in the hexagonal ZrBeSi structure type, while changing the post-transition metal causes CsCdSb and RbCdSb to arrange in the tetragonal PbFCl structure type. Synthesis, crystal structures, stability, and calculated electronic band structures for these compounds are discussed herein. The band inversion of CsCdSb and RbCdSb is explored and indicates potential topologically interesting properties.

Results and Discussion

Crystal Structure of AZnSb (A = Rb, Cs)

*A*ZnSb (*A* = Rb, Cs) crystallizes in the hexagonal space group $P6_3/mmc$ (No. 194, $Z = 2$) in the ZrBeSi structure type, an ordered variant of the well-known AlB_2 structure type (Figure 1). CsZnSb/RbZnSb have unit cell dimensions of $a = 4.5588(2)/4.5466(4)$ Å and $c = 11.9246(6)/11.0999(10)$ Å (Table 1). These structures have three unique positions within the unit cell (Table 2). The structure is built from flat hexagonal graphene-like layers of Zn_3Sb_3 that are stacked along the *c*-axis, with the alkali metal sitting at the center of the hexagonal prisms formed by two Zn_3Sb_3 rings from adjoining layers. Additional refinement details and anisotropic parameters are presented in Tables 1-3.

* Dr. Bryan Owens-Baird, Shannon Lee, Prof. Dr. Kirill Kovnir
E-mail: kovnir@iastate.edu
[a] Department of Chemistry
Iowa State University
Ames, Iowa 50011, United States
Dr. Bryan Owens-Baird, Dr. Lin-Lin Wang, Shannon Lee, Prof. Dr. Kirill Kovnir
[b] Ames Laboratory
U.S. Department of Energy
Ames, Iowa 50011, United States

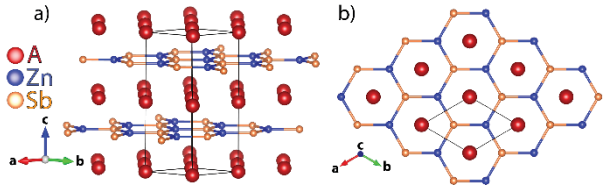

Figure 1. The crystal structure of *A*ZnSb (*A* = Rb, Cs): a) perspective view; and b) view along the *c*-axis (Rb/Cs: red, Zn: blue, Sb: orange). Unit cell is shown as black lines.

To date, the ZrBeSi structure type has been well represented in the literature with numerous examples, such as: LiBC, *Ae*M*Pn* (*Ae* = Ca, Sr, Ba, Eu; *M* = Cu, Ag, Au; *Pn* = P, As, Sb), *Ae*LiP (*Ae* = Sr, Ba), KZn*Pn* (*Pn* = P, As, Sb), K*M*Te (*M* = Cu, Au), and KHg*Pn* (*Pn* = As, Sb) to name a few.[23-38] Additionally, the flat hexagonal layer can be found in more complex structures, such as the layered $NaCu_{6.3}Sb_3$ compound.[39] Furthermore, there are also examples of structures that deviate slightly from this structure type by a puckering of the hexagonal layer, like in the case of LiZnSb.[40] This structure type has gained notoriety since the discovery of the superconductivity in MgB_2.[41] Interestingly, in contradiction with our experimental observations, the computational report that predicted RbZnSb to be energetically favorable, predicted it to crystallize in the LiYSn structure, which is a disordered version of the ZrBeSi structure type.[22]

When comparing the unit cells of *A*ZnSb (*A* = K, Rb, Cs) compounds crystallizing in the ZrBeSi structure type, an interesting trend becomes apparent: the *a* parameter of the cell is relatively independent of the size of the alkali metal situated between the layers. KZnSb, RbZnSb, and CsZnSb compounds have *a* lattice parameters of 4.54 Å, 4.55 Å, and 4.56 Å, respectively.[34] Instead, we find that all expansion of the unit cell is directionalized along the *c* parameter that corresponds to the interlayer direction; 10.50 Å, 11.10 Å, and 11.92 Å for KZnSb, RbZnSb, and CsZnSb, respectively. This indicates that ZnSb layer defines the in-plane unit cell parameters and further expansion of the covalent Zn-Sb bonds is energetically unfavorable. This non-expansion of the *a* parameter with changing cation size appears to be a unique trend within this subset of materials when compared to known systems. For instance, in the *Ae*CuSb (*Ae* = Ca, Sr, Ba), the *a* parameter increases from 4.45 Å to 4.52 Å to 4.61 Å for Ca-Sr-Ba compounds.[26,29]

Zn-Sb distances within the Zn_3Sb_3 layers are 2.625(1) Å and 2.632(1) Å for RbZnSb and CsZnSb, respectively, and are comparable to the sum of the two covalent radii (2.61 Å; r_{Zn} = 1.22 Å; r_{Sb} = 1.39 Å),[42] and Zn-Sb distances in isostructural KZnSb (2.621 Å) and puckered layered LiZnSb (2.687 Å).[34,40] Other *A*-Zn-Sb compounds on the other hand tend to have slightly longer Zn-Sb distances; 2.694 Å for the $Cs_8Zn_{18}Sb_{28}$ clathrate, 2.720 Å for $Rb_2Zn_5Sb_4$, 2.769 Å for NaZnSb, and 2.802 Å for Li_2ZnSb.[34, 43-45]

Crystal Structure of ACdSb (A = Rb, Cs)

Interestingly, when examining the Cd-analogues, we find that the observed structure has changed. *A*CdSb (*A* = Rb, Cs) crystallize in the tetragonal *P*4/*nmm* space group (No. 129; *Z* = 2) in the PbFCl structure type (Figure 2).[46] CsCdSb/RbCdSb have lattice parameters of *a* = 4.8884(5)/4.8227(3) Å and *c* = 8.8897(9)/8.5492(7) Å. Like their hexagonal Zn counterparts, the Cd structures have three unique crystallographic sites (Table 2). *A*CdSb (*A* = Rb, Cs) are layered structures, with alkali metal sandwiched between Cd_2Sb_2 slabs. These Cd_2Sb_2 slabs are composed by a square net of Cd atoms that are alternately capped by Sb atoms, with the alkali metal sitting opposite to the Sb capped position. Alkali cations are situated in the center of square prisms formed by eight Sb atoms. Additional refinement details and anisotropic parameters can be found in Tables 1-3.

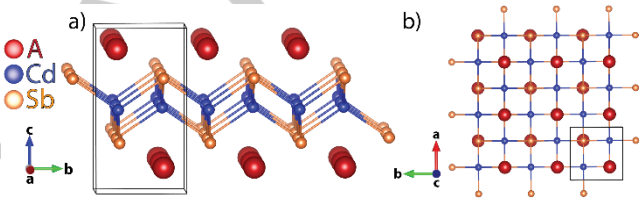

Figure 2. The crystal structure of *A*CdSb (*A* = Rb, Cs): a) perspective view; and b) view along the *c*-axis (Rb/Cs: red, Cd: blue, Sb: orange). Unit cell is shown as black lines.

The PbFCl structure type is also quite common, with examples spanning much of the periodic table and include many compounds that do not contain electropositive alkali or alkaline-earth metals. There are still numerous examples of compounds that are similar to the presented compounds, *A*Mn*Pn* (*A* = Li, Na, K, Rb, Cs; *Pn* = P, As, Sb, Bi), NaZn*Pn* (*Pn* = P, As, Sb), and NaAl*Tr* (*Tr* = Si, Ge) to name a few.[47-55] The analogues of Cd_2Sb_2 layers are also found in many notable systems, for instance in the Fe-based superconducting systems: FeSe, $BaFe_2As_2$, and isostructural LiFeAs etc.[56-60] While many isostructural examples are present, we found only two other Cd-containing examples: KCd*Pn* (*Pn* = As, Sb).[61]

The observed Cd-Sb distances within the layers are 2.9566(8) Å and 2.9611(5) Å for RbCdSb and CsCdSb, respectively, which is significantly longer than the sum of their covalent radii (2.83 Å; r_{Cd} = 1.44 Å; r_{Sb} = 1.39 Å).[42] Contrasting, in the isostructural KCdSb much shorter Cd-Sb distances of 2.858 Å are present.[61] Longer Cd-Sb distances can be found in alkaline-earth zinc-antimonides, $K_2SrCdSb_2$ (2.93-3.09 Å), $Ba_3Cd_2Sb_4$ (2.91-2.95 Å), $BaCdSb_2$ (2.92 Å).[62-64]

Composition of all phases was further confirmed through energy dispersive X-ray spectroscopy, corroborating the SC-XRD results. The following compositions have been normalized to one alkali metal: $CsZn_{1.03(2)}Sb_{1.03(3)}$, $RbZn_{1.04(6)}Sb_{1.04(6)}$, $CsCd_{1.01(1)}Sb_{0.99(1)}$, and $RbCd_{1.02(3)}Sb_{1.00(3)}$.

Synthesis and Calorimetry

The synthesis of all title compounds can be achieved through a stoichiometric reaction of the elements. PXRD patterns taken of the samples are shown in Figure 3. Noise and additional features seen in Figures 3b and 3d are due to the subtraction of the air-sensitive holder background. To offset the high vapor pressure of the alkali metals at high-temperatures, the samples were welded shut within Ta ampoules before sealing into fused silica tubes. For full homogenization of the samples multiple annealings at 823 K, with grinding in between, must be employed. The synthetic temperature plays a crucial role in the products obtained. If a temperature above 823 K is used, the collected products become amorphous or other compounds with different stoichiometries form (not discussed here). When the temperature is increased to approximately 873-923 K, reaction with the Ta vessel occurs and Ta_3Sb can be found in the products. On the other hand, lower than 823 K temperatures result in inadequate mixing and multiphase samples.

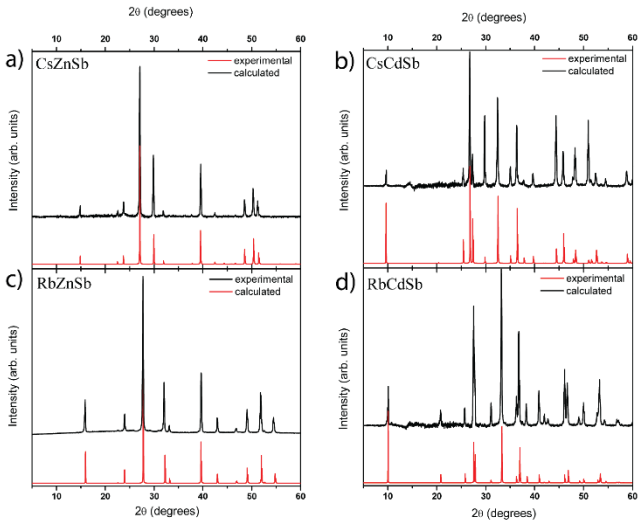

Figure 3. Powder X-ray diffraction patterns for: a) CsZnSb, b) CsCdSb, c) RbZnSb, and d) RbCdSb (λ = 1.5406 Å). Experimental pattern shown in black, while red is the calculated pattern. The background from the air-sensitive holder has been subtracted for clarity in b) and d) creating background wiggles in the 12-18° 2θ range.

Both *A*ZnSb and *A*CdSb systems are air- and water-sensitive, though the Cd-based compounds to a much greater degree. Immediate removal from an inert atmosphere results in a decomposition of the *A*CdSb phases, seen by PXRD. *A*ZnSb compounds on the other hand are stable for a short period of time (~30 min.) at ambient conditions before noticeable degradation is detected by PXRD.

Differential scanning calorimetry (DSC) measurements were performed for the *AM*Sb (*A* = Rb, Cs; *M* = Zn, Cd) compounds (Figure 4). All four compounds show a broad endothermic peak upon heating, indicating either melting or decomposition. Onset temperatures are 975 K (CsZnSb), 1040 K (RbZnSb), 1060 K (CsCdSb), and 1057 K (RbCdSb). DSC ampoules after these experiments were highly discolored, indicating reaction of alkali metal with silica. PXRD of the samples after DSC show no trace of the original title compounds. Though peaks are seen in the cooling plots for the *A*CdSb samples, only amorphous material remained according to PXRD. In turn, $Rb_2Zn_5Sb_4$ and a small number of unidentifiable peaks are found for RbZnSb, in line with the depletion of sample with Rb due to reaction with ampoule walls; while the PXRD peaks from the CsZnSb DSC sample cannot be assigned to known crystalline phases. To probe whether these decomposition products are due to the incongruent melting of the sample or to reaction with the silica ampoule, *AM*Sb samples were sealed within Ta ampoules and quickly annealed (15 min.) above their respective endothermic peak temperature. Unfortunately, all compounds reacted with the Ta ampoule during this timeframe, resulting in PXRD patterns containing Ta_3Sb and amorphous products.

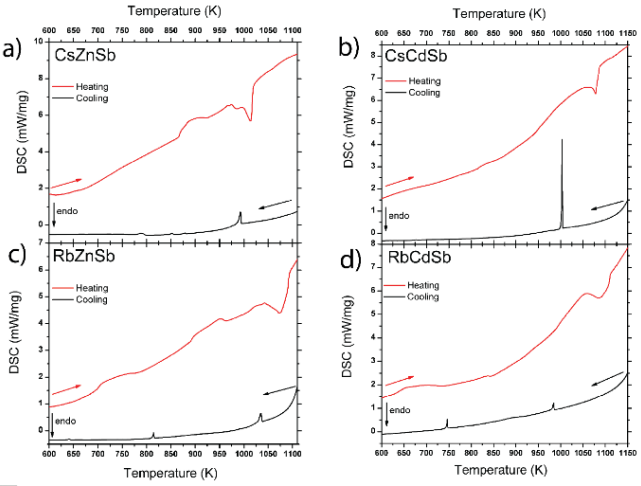

Figure 4. DSC plots for: a) CsZnSb, b) CsCdSb, c) RbZnSb, and d) RbCdSb. The unlabeled arrows indicate the direction of measurement.

Electronic Band Structure Calculations

Figure 5 shows the electronic band structures of the title compounds, which have been calculated in density functional theory (DFT) with PBE as exchange-correlation functional and included spin-orbit coupling (SOC) interactions.[65-67] Because some compounds in the ZrBeSi or PbFCl structure types have shown interesting topologically properties,[16-21] we will discuss the band inversion features in detail. In Figure 5, potential band inversion is shown by the projection of Zn/Cd *s* orbitals (green dots) on the bands. KHgSb compound, which also crystalizes in ZrBeSi structure type, was first predicted as topologically trivial. A later study found it hosts hourglass surface states, a topologically non-trivial behavior protected by glide planes, one of the non-symmorphic symmetries.[17,20] For this to happen, the bands derived from Hg-6*s* orbitals need to be inverted below the valence band, so both the conduction and valence bands are derived from

Sb-5*p* orbitals. In contrast, CsZnSb (Figure 5a) and RbZnSb (Figure 5c) have no such band inversion. The bands derived from Zn-4*s* orbitals remain as the conduction band along $\Gamma - A$ direction, similar to that in KZnP. Thus, they are topologically trivial with a narrow band gap around 0.3 eV. For the PbFCl structure type, ZrSiS and related compounds host nodal line loops without SOC and become weak topological insulators with Dirac-like dispersion when SOC gaps out the nodal line loops.[16] In CsCdSb (Figure 5b) and RbCdSb (Figure 5d), there is an interesting band inversion along $\Gamma - Z$ direction, with bands derived from Cd-5*s* orbitals being inverted below the valence band. But the exact topological properties are not clear and demand further analysis.

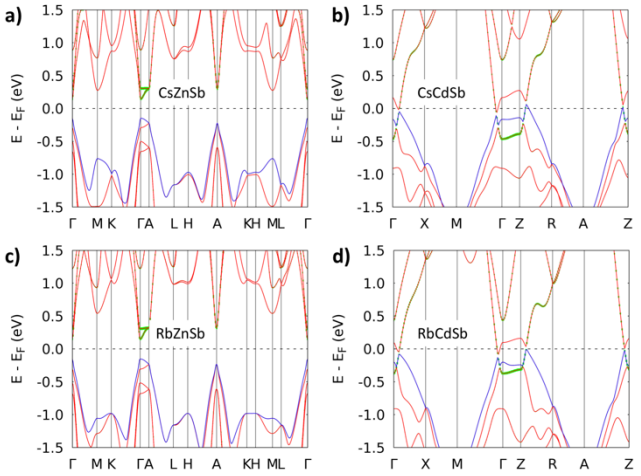

Figure 5. Electronic band structure calculated in DFT with PBE+SOC for (a) CsZnSb, (b) CsCdSb, (c) RbZnSb and (d) RbCdSb. The valence band is plotted in blue and projection of Zn/Cd *s* orbitals are highlighted as green dots.

Conclusion

Four new ternary metal antimonides *AM*Sb (*A* = Rb, Cs; *M* = Zn, Cd) have been synthesized in the form of single-phase samples. Crystal structure determination using single-crystal X-ray diffraction shows that Zn-containing phases crystallize in ZrBeSi structure type, while the Cd phases crystallize in the PbFCl structure type. All compounds are air- and moisture-sensitive. DSC and subsequent PXRD measurements show that all phases decompose between 975 K and 1060 K, with the detectable reaction between melt and silica DSC vessels at high-temperatures. Analysis of the electronic band structure shows that Zn-containing antimonides are topologically trivial, while Cd-containing compounds exhibit a band inversion along $\boldsymbol{\Gamma - Z}$ direction.

Experimental Section

Synthesis: Handling and manipulation of starting materials and products was carried out in an argon filled glovebox ($p(O_2) < 0.1$ ppm). All chemicals were used as received from Alfa Aesar: Cs metal (99.8%), Rb metal (99.75%), Zn granules (99.8%), Cd shot (99.95%), and Sb shot (99.999%).

All samples were synthesized via reaction of the elements. Stoichiometric amounts of starting materials were loaded into Ta ampoules that were welded shut under argon atmosphere. The Ta ampoules were enclosed into silica ampules, which were evacuated, and flame sealed. The ampoules were heated from room temperature to 823 K over 10 h, annealed for 120 h, and cooled to room temperature naturally. Samples were ground and reannealed under the same conditions two additional times to ensure homogeneity, producing light-gray powder. Single-phase samples were collected for each composition (Figure 3).

Powder X-ray Diffraction: Samples were analyzed via room-temperature powder X-ray diffraction using a Rigaku Miniflex 600 diffractometer employing Cu-K_α radiation (λ = 1.54185 Å) with a Ni-K_β filter. CsZnSb and RbZnSb scans were performed from 5 – 60° 2θ on a spinning Si-crystal zero-background plate on air, while CsCdSb and RbCdSb scans were performed on a home-made spinning air-free holder with a Kapton lid.

Single-Crystal X-ray Diffraction: Single-Crystal X-ray Diffraction was carried out using a Bruker D8 Venture diffractometer with a Bruker Photon100 CMOS detector employing Mo-K_α radiation (λ = 0.71073 Å). The dataset was collected at 100 K under a N_2 stream with a variety of φ- and ω-scans recorded at a 0.3° step and integrated using the Bruker SAINT software package.[68] Multiscan absorption correction was used. Structure solution and refinement was achieved using the SHELX suite.[69] Atomic positions, occupancy, and equivalent atomic displacement parameters for *AM*Sb (*A* = Rb, Cs; *M* = Zn, Cd) are shown in Table 2. Full details of the structure refinement and anisotropic displacement parameters can be found in Tables 1 and 3.

Energy Dispersive X-ray Spectroscopy: Elemental composition analysis was performed through Energy Dispersive X-ray Spectroscopy using a FEI Quanta 250 field emission-SEM with EDS detection (Oxford X-Max 80) and Aztec software. Powders and crystals were mounted onto Al stubs on conductive carbon tape in an air-sensitive holder. The electron beam energy used was held constant at 15eV with a working distance of 10.5 mm. For each composition, measurements were taken at a collection of sites to improve statistics.

Differential Scanning Calorimetry: Differential Scanning Calorimetry was performed using a 404 F1 Pegasus calorimeter (Netzsch Thermal Analysis). Approximately 30 mg of sample was loaded in silica ampoules, which were evacuated and sealed. The DSC measurements were performed between 300-1170 K with a heating/cooling rate of 10 K/min.

Electronic Band Structure Calculations: Band structure with spin-orbit coupling (SOC) in density functional theory (DFT) have been calculated with PBE exchange-correlation functional, a plane-wave basis set and projected augmented wave method as implemented in VASP.[65-67, 70-72] For ZrBeSi and PbFCl structure-types, the Monkhorst-Pack *k*-point mesh of (12×12×5) and (11×11×6) including the Γ point have been used, respectively.[73] A kinetic energy cutoff of 277 eV has been used to expand the plane-wave coefficients.

Table 1. Single crystal data and refinement parameters for *AM*Sb at 100 K.

empirical formula	**CsZnSb**	**RbZnSb**	**CsCdSb**	**RbCdSb**
CCDC-number	1963959	1963962	1963960	1963961
temperature	100(2) K			
radiation, λ	Mo-K$_\alpha$, 0.71073 Å			
crystal system	hexagonal		tetragonal	
space group	$P6_3/mmc$ (No. 194)		P_4/nmm (No. 129)	
a, Å	4.5588(2)	4.5466(4)	4.8884(5)	4.8227(3)
c, Å	11.9246(6)	11.0999(10)	8.8897(9)	8.5492(7)
Volume, Å^3	214.62(2)	198.71(4)	212.43(5)	198.84(3)
Z	2	2	2	2
Data/param.	157/8	113/7	177/10	211/9
dens., g/cm^3	4.95	4.56	5.74	5.34
μ, mm^{-1}	19.998	24.739	19.564	24.039
R_{int}	0.032	0.068	0.033	0.082
Good.-of-fit	1.12	1.50	1.41	1.37
R_1 [$I > 2\sigma(I)$]	0.011	0.020	0.017	0.025
wR_2 [$I > 2\sigma(I)$]	0.022	0.036	0.037	0.076
R_1 [all data]	0.014	0.027	0.017	0.036
wR_2 [all data]	0.023	0.038	0.037	0.079
Diff. peaks, eÅ^{-3}	0.91/-0.57	0.73/-1.65	1.89/-1.09	1.04/-1.87

Table 2. Atomic coordinates and equivalent atomic displacement parameters of *AM*Sb at 100 K.

Atom	Wyckoff	*x/a*	*y/b*	*z/c*	Occup.	U_{eq} (Å^2)[a]
CsZnSb						
Cs	2*a*	0	0	½	1	0.009(1)
Zn	2*d*	⅔	⅓	½	1	0.007(1)
Sb	2*c*	⅔	⅓	¾	1	0.007(1)
RbZnSb						
Rb	2*a*	0	0	½	1	0.005(1)
Zn	2*c*	⅔	⅓	¾	1	0.009(1)
Sb	2*d*	⅓	⅔	¾	1	0.007(1)
CsCdSb						
Cs	2*c*	¼	¼	0.8513(7)	1	0.009(1)
Cd	2*b*	¾	¼	½	1	0.006(1)
Sb	2*c*	½	½	0.31198(8)	1	0.008(1)
RbCdSb						
Rb	2*c*	¼	¼	0.8483(2)	1	0.009(1)
Cd	2*b*	¾	¼	½	1	0.007(1)
Sb	2*c*	¾	¾	0.7001(2)	1	0.005(1)

[a] U_{eq} is defined as one third of the trace of the orthogonalized U_{ij} tensor

Table 3. Anisotropic displacement parameters (Å^2) of *AM*Sb at 100 K.[a]

Atom	U_{11}	U_{22}	U_{33}	U_{12}	U_{13}	U_{23}
CsZnSb						
Cs	0.010(1)	0.010(1)	0.008(1)	0	0	0.005(1)
Zn	0.006(1)	0.006(1)	0.009(1)	0	0	0.003(1)
Sb	0.004(1)	0.005(1)	0.011(1)	0	0	0.002(1)
RbZnSb						
Rb	0.009(1)	0.009(1)	0.010(1)	0	0	0.002(1)
Zn	0.006(1)	0.006(1)	0.010(1)	0	0	0.003(1)
Sb	0.003(1)	0.003(1)	0.010(1)	0	0	0.003(1)
CsCdSb						
Cs	0.009(1)	0.009(1)	0.010(1)	0	0	0
Cd	0.007(1)	0.007(1)	0.008(1)	0	0	0
Sb	0.005(1)	0.005(1)	0.009(1)	0	0	0
RbCdSb						
Rb	0.006(1)	0.006(1)	0.014(1)	0	0	0
Cd	0.005(1)	0.005(1)	0.011(1)	0	0	0
Sb	0.004(1)	0.004(1)	0.010(1)	0	0	0

[a] The anisotropic displacement factor exponent takes the form: $-2\pi^2[h^2a^{*2}U_{11} + \ldots + 2hka^*b^*U_{12}]$.

Acknowledgements

We would like to thank Prof. J. Zaikina (ISU) for access to the arc-welder. This work was supported by the Laboratory Research and Development Program of the Ames Laboratory under the U.S. Department of Energy Contract DE-AC02-07CH11358. B.O.B acknowledges partial support form Center for Catalysis (CCAT) at Iowa State University. L.-L.W. was supported by the Center for the Advancement of Topological Semimetals, an Energy Frontier Research Center funded by the U.S. DOE, Office of Basic Energy Sciences.

Keywords: Antimonides • Synthesis • Crystal Structure • Electronic Structure • Band Inversion

1. H. Kleinke, *Chem. Soc. Rev.* **2000,** *29* (6), 411-418.
2. J. Wang, K. Kovnir, *J. Am. Chem. Soc.* **2015,** *137* (39), 12474-12477.
3. A. S. Mikhaylushkin, J. Nylén, U. Häussermann, *Chem. Eur. J.* **2005,** *11* (17), 4912-4920.
4. A. M. Mills, R. Lam, M. J. Ferguson, L. Deakin, A. Mar, *Coord. Chem. Rev.* **2002,** *233-234*, 207-222.
5. T. Cox, V. Gvozdetskyi, B. Owens-Baird, J. V. Zaikina, *Chem. Mater.* **2018,** *30* (23), 8707-8715.
6. V. Gvozdetskyi, B. Owens-Baird, S. Hong, T. Cox, G. Bhaskar, C. Harmer, Y. Sun, F. Zhang, C.-Z. Wang, K.-M. Ho, J. V. Zaikina, *Chem. Mater.* **2019**.
7. B. R. Bennett, R. Magno, J. B. Boos, W. Kruppa, M. G. Ancona, *Solid State Electon.* **2005,** *49* (12), 1875-1895.
8. J. A. del Alamo, *Nature* **2011,** *479* (7373), 317-323.
9. D. Li, C. Lan, A. Manikandan, S. Yip, Z. Zhou, X. Liang, L. Shu, Y.-L. Chueh, N. Han, J. C. Ho, *Nat. Commun.* **2019,** *10* (1), 1664.
10. H. Kleinke, *Chem. Mater.* **2010,** *22* (3), 604-611.
11. G. J. Snyder, E. S. Toberer, *Nat. Mater.* **2008,** *7* (2), 105-114.
12. S. R. Brown, S. M. Kauzlarich, F. Gascoin, G. J. Snyder, *Chem. Mater.* **2006,** *18* (7), 1873-1877.
13. Y. Hu, G. Cerretti, E. L. Kunz Wille, S. K. Bux, S. M. Kauzlarich, *J. Solid State Chem.* **2019,** *271*, 88-102.
14. Robert W. McKinney, P. Gorai, S. Manna, E. Toberer, V. Stevanović, *J. Mater. Chem. A* **2018,** *6* (32), 15828-15838.
15. ICSD, **2017,** *Version 1.9.9, 2017-1*.
16. L. M. Schoop, M. N. Ali, C. Straßer, A. Topp, A. Varykhalov, D. Marchenko, V. Duppel, S. S. P. Parkin, B. V. Lotsch, C. R. Ast, *Nat. Commun.* **2016,** *7*, 11696.
17. Z. Wang, A. Alexandradinata, R. J. Cava, B. A. Bernevig, *Nature* **2016,** *532*, 189.
18. Q. Xu, Z. Song, S. Nie, H. Weng, Z. Fang, X. Dai, *Phys. Rev. B* **2015,** *92* (20), 205310.
19. Q. D. Gibson, L. M. Schoop, L. Muechler, L. S. Xie, M. Hirschberger, N. P. Ong, R. Car, R. J. Cava, *Phys. Rev. B* **2015,** *91* (20), 205128.
20. H.-J. Zhang, S. Chadov, L. Müchler, B. Yan, X.-L. Qi, J. Kübler, S.-C. Zhang, C. Felser, *Phys. Rev. Lett.* **2011,** *106* (15), 156402.
21. L. M. Schoop, F. Pielnhofer, B. V. Lotsch, *Chem. Mater.* **2018,** *30* (10), 3155-3176.
22. X. Zhang, L. Yu, A. Zakutayev, A. Zunger, *Adv. Funct. Mater.* **2012,** *22* (7), 1425-1435.
23. W. Bronger, H. U. Kathage, *J. Less-Common Met.* **1990,** *160* (1), 181-184.
24. W. Bronger, H. U. Kathage, *J. Alloys Compd.* **1992,** *184* (1), 87-94.
25. Y. Dong, F. J. DiSalvo, *J. Solid State Chem.* **2007,** *180* (2), 432-439.
26. B. Eisenmann, G. Cordier, H. Schaefer, *Z. Naturforsch* **1974,** *29b*, 457-459.
27. D. Johrendt, R. Miericke, A. Mewis, *Z. Naturforsch* **1996,** *51b*, 905-906.
28. E. K. Lee, G. J. Miller, S. K. Kang, *Acta Crystallogr. E* **2002,** *58* (2), i17-i18.
29. F. Merlo, M. Pani, M. L. Fornasini, *J. Less-Common Met.* **1990,** *166* (2), 319-327.
30. A. Mewis, *Z. Naturforsch* **1978,** *33b*, 983-986.
31. A. Mewis, *Z. Naturforsch* **1979,** *34b*, 1373-1376.
32. T. Mishra, I. Schellenberg, M. Eul, R. Pöttgen, Structure and properties of EuTSb (T = Cu, Pd, Ag, Pt, Au) and YbIrSb. In *Z. Kristallogr. Cryst. Mater.*, 2011; Vol. 226, p 590.
33. J. Nuss, M. Jansen, *Z. Anorg. Allg. Chem.* **2009,** *635* (11), 1514-1516.
34. G. Savelsberg, H. Schafer, *Z. Naturforsch* **1978,** *33b*, 370-373.
35. W. Tomuschat, H. U. Schuster, *Z. Naturforsch* **1981,** *36b*, 1193-1194.
36. P. Vogel, H. U. Schuster, *Z. Naturforsch* **1980,** *35b*, 114-116.
37. M. Wörle, R. Nesper, G. Mair, M. Schwarz, H. G. Von Schnering, *Z. Anorg. Allg. Chem.* **1995,** *621* (7), 1153-1159.
38. J. W. Nielsen, N. C. Baenziger, *Acta Crystallogr.* **1954,** *7* (1), 132-133.
39. B. Owens-Baird, S. Lee, K. Kovnir, *Dalton Trans.* **2017,** *46* (37), 12438-12445.
40. H. U. Schuster, G. Schroeder, *Z. Naturforsch* **1972,** *27b*, 81-82.
41. J. Nagamatsu, N. Nakagawa, T. Muranaka, Y. Zenitani, J. Akimitsu, *Nature* **2001,** *410* (6824), 63-64.
42. B. Cordero, V. Gomez, A. E. Platero-Prats, M. Reves, J. Echeverria, E. Cremades, F. Barragan, S. Alvarez, *Dalton Trans.* **2008,** (21), 2832-2838.
43. H. He, S. S. Stoyko, A. Mar, S. Bobev, *Acta Crystallogr. C* **2013,** *69* (5), 455-459.
44. Y. Liu, L.-M. Wu, L.-H. Li, S.-W. Du, J. D. Corbett, L. Chen, *Angew. Chem. Int. Ed.* **2009,** *48* (29), 5305-5308.
45. G. Schroeder, H.-U. Schuster, *Z. Anorg. Allg. Chem.* **1977,** *431* (1), 217-220.
46. W. B. Pearson, The Cu_2Sb and related structures. In *Z. Kristallogr. Cryst. Mater.*, 1985; Vol. 171, p 23.
47. V. Gvozdetskyi, B. Owens-Baird, S. Hong, J. V. Zaikina, *Materials* **2018,** *12* (1), 48.
48. G. Achenbach, H.-U. Schuster, *Z. Anorg. Allg. Chem.* **1981,** *475* (4), 9-17.
49. W. Bronger, P. Müller, R. Höppner, H.-U. Schuster, *Z. Anorg. Allg. Chem.* **1986,** *539* (8), 175-182.
50. L. Lompwsky, W. Bronger, *Z. Anorg. Allg. Chem.* **1974,** *409* (2), 221-227.
51. R. Müller, M. Kuckel, H.-U. Schuster, P. Müller, W. Bronger, *J. Alloys Compd.* **1991,** *176* (1), 167-172.
52. F. Schucht, A. Dascoulidou, R. Müller, W. Jung, H.-U. Schuster, W. Bronger, P. Müller, *Z. Anorg. Allg. Chem.* **1999,** *625* (1), 31-36.
53. H. Kahlert, H. U. Schuster, *Z. Naturforsch* **1976,** *31b*, 1538-1539.
54. B. Eisenmann, M. Somer, *Z. Naturforsch* **1985,** *40b*, 1419-1423.
55. W. Westerhaus, H. U. Schuster, *Z. Naturforsch* **1979,** *34b*, 352-353.
56. F.-C. Hsu, J.-Y. Luo, K.-W. Yeh, T.-K. Chen, T.-W. Huang, P. M. Wu, Y.-C. Lee, Y.-L. Huang, Y.-Y. Chu, D.-C. Yan, M.-K. Wu, *Proc. Natl. Acad. Sci. U.S.A.* **2008,** *105* (38), 14262-14264.
57. M. Rotter, M. Tegel, D. Johrendt, *Phys. Rev. Lett.* **2008,** *101* (10), 107006.
58. M. Shatruk, *J. Solid State Chem.* **2019,** *272*, 198-209.
59. M. J. Pitcher, D. R. Parker, P. Adamson, S. J. C. Herkelrath, A. T. Boothroyd, R. M. Ibberson, M. Brunelli, S. J. Clarke, *Chem. Commun.* **2008,** (45), 5918-5920.
60. J. H. Tapp, Z. Tang, B. Lv, K. Sasmal, B. Lorenz, P. C. W. Chu, A. M. Guloy, *Phys. Rev. B* **2008,** *78* (6), 060505.
61. H. Kahlert, H. U. Schuster, *Z. Naturforsch* **1976,** *31b*, 1538-1539.
62. E. Brechtel, G. Cordier, H. Schäfer, *J. Less-Common Met.* **1981,** *79* (1), 131-138.
63. B. Saparov, M. Saito, S. Bobev, *J. Solid State Chem.* **2011,** *184* (2), 432-440.
64. B. Saparov, S.-Q. Xia, S. Bobev, *Inorg. Chem.* **2008,** *47* (23), 11237-11244.
65. P. Hohenberg, W. Kohn, *Phys. Rev.* **1964,** *136* (3B), B864-B871.
66. W. Kohn, L. J. Sham, *Phys. Rev.* **1965,** *140* (4A), A1133-A1138.
67. J. P. Perdew, K. Burke, M. Ernzerhof, *Phys. Rev. Lett.* **1996,** *77* (18), 3865-3868.
68. W. Bruker AXS Inc.: Madison, USA, **2007**.
69. G. Sheldrick, *Acta Ctrystallogr. A* **2008,** *64* (1), 112-122.
70. P. E. Blöchl, *Phys. Rev. B* **1994,** *50* (24), 17953-17979.
71. G. Kresse, J. Furthmüller, *Comp. Mater. Sci.* **1996,** *6* (1), 15-50.
72. G. Kresse, J. Furthmüller, *Phys. Rev. B* **1996,** *54* (16), 11169-11186.
73. H. J. Monkhorst, J. D. Pack, *Phys. Rev. B* **1976,** *13* (12), 5188-5192.

Entry for the Table of Contents

FULL PAPER

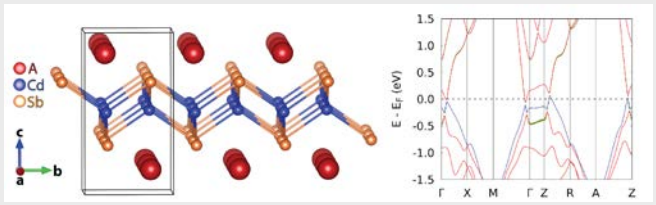

Crystal structure of new CsCdSb compound crystallizing in PbFCl structure type is shown together with calculated band structure showing potential band inversion.

*Bryan Owens-Baird, Lin-Lin Wang, Shannon Lee, and Kirill Kovnir**

Page No. – Page No.

Synthesis, Crystal and Electronic Structure of Layered *AM*Sb Compounds (*A* = Rb, Cs; *M* = Zn, Cd)

Additional Author information for the electronic version of the article.

Kirill Kovnir: 0000-0003-1152-1912
Bryan Owens-Baird: 0000-0003-3128-5363
Lin-Lin Wang: 0000-0003-0965-3246
Shannon Lee: 0000-0002-7541-3286